Chicken HOXA3 Gene: Its Expression Pattern and Role in Branchial Nerve Precursor Cell Migration

AUTHOR(S):

Watari-Goshima, Natsuko; Osamu, Chisaka

CITATION:

Watari-Goshima, Natsuko ...[et al]. Chicken HOXA3 Gene: Its Expression Pattern and Role in Branchial Nerve Precursor Cell Migration. International Journal of Medical Sciences 2011, 7: 87-101

ISSUE DATE:

2011-01-19

URL:

http://hdl.handle.net/2433/139442

International Journal of Biological Sciences
2011; 7(1):87-101

Research Paper

Chicken HOXA3 Gene: Its Expression Pattern and Role in Branchial Nerve Precursor Cell Migration

Natsuko Watari-Goshima[1*] and Osamu Chisaka[2] ✉

1. Department of Biophysics, Graduate School of Science, Kyoto University, Sakyo-ku, Kyoto 606-8501, Japan
2. Department of Cell and Developmental Biology, Graduate School of Biostudies, Kyoto University, Sakyo-ku, Kyoto 606-8501, Japan

* Present address: 3-12-69-2-233, Yada, Higashi-ku, Nagoya 461-0040, Japan

✉ Corresponding author: Osamu Chisaka, Ph.D., Dept. of Cell and Developmental Biology, Graduate School of Biostudies, Kyoto University, Yoshidakonoe-cho, Sakyo-ku, Kyoto 606-8501, Japan. Phone 81 (75) 753-9239; Fax 81 (75) 753-4265; e-mail: chisaka@lif.kyoto-u.ac.jp

Received: 2010.09.09; Accepted: 2011.01.17; Published: 2011.01.19

Abstract

In vertebrates, the proximal and distal sensory ganglia of the branchial nerves are derived from neural crest cells (NCCs) and placodes, respectively. We previously reported that in *Hoxa3* knockout mouse embryos, NCCs and placode-derived cells of the glossopharyngeal nerve were defective in their migration. In this report, to determine the cell-type origin for this *Hoxa3* knockout phenotype, we blocked the expression of the gene with antisense morpholino oligonucleotides (MO) specifically in either NCCs/neural tube or placodal cells of chicken embryos. Our results showed that *HOXA3* function was required for the migration of the epibranchial placode-derived cells and that *HOXA3* regulated this cell migration in both NCCs/neural tube and placodal cells. We also report that the expression pattern of chicken *HOXA3* was slightly different from that of mouse *Hoxa3*.

Key words: *Hoxa3*, branchial nerve, neural crest, placode, axon guidance, hindbrain, cell migration

Introduction

Vertebrate *Hox* genes encode helix-turn-helix transcription factors that are orthologs of the invertebrate homeotic selector gene complex (HOM-C), which defines segmental identities of each hemisegment of the body [1]. These *Hox* genes are known to have crucial roles in embryonic body patterning along the anterior-posterior (A-P) and proximal-distal (P-D) axes. There are 39 known *Hox* genes in mice and humans, and they are located in 4 gene clusters, one on each of 4 chromosomes [2].

The developing vertebrate hindbrain transiently forms metameric structures called rhombomeres [3], in which cell movement is restricted for a certain period during development [4]. The even-numbered rhombomeres further develop specific cranial nerves [5]. This unique feature of rhombomeres provides a good model for studying the A-P patterning mechanisms of the vertebrate brain. NCCs which arise from the dorsal edge of the rhombomeres, also convey the A-P identities of the neural tube in which they originate; and they migrate in segmental streams to the branchial arches to form mesenchyme, some connective tissues, bones, thyroid, parathyroid, sensory cranial neurons, Schwann cells, etc. (reviewed in [6-8]). Some *Hox* genes have their anterior expression borders at a certain rhombomere boundary, and are also expressed in NCCs. The combination of *Hox* genes expressed in these rhombomeres or NCCs (Hox code; [9]) is important for defining A-P identities of these cells, and there are numbers of *Hox* gene knockout mice that show hindbrain or laryngeal region defects ([10] and references therein).

Hoxa3 is a group 3 paralog member of the *Hox* gene family and has pleiotropic functions in organogenesis around the hindbrain and branchial arch regions of mouse embryos [10-17]. Most of the affected organs of *Hoxa3* knockout mice, e.g., thymus, thyroid, parathyroid, heart valves, third branchial arch artery, glossopharyngeal nerve (IXth nerve), etc. partially originate from NCCs; and this knockout mouse phenotype quite resembles that of the human disease called DiGeorge syndrome [11].

The IXth nerve is a branchial nerve. Branchial nerves, i.e., the trigeminal (Vth), facial (VIIth), glossopharyngeal (IXth), and vagus (Xth), consist of motor nuclei in the brain stem and sensory ganglia located lateral to the neural tube. Sensory neurons of the Vth nerve in the trigeminal ganglion are derived from both NCCs and the trigeminal placode. Sensory neurons in the proximal ganglia of the other branchial nerves are derived from NCCs; and the neurons in the distal ganglia (i.e., the geniculate, petrosal, and nodose ganglion of the VIIth, IXth, and Xth nerve, respectively) are derived from epibranchial placode cells [18]. The molecular mechanisms regulating the migration and axon guidance of these neuronal precursor cells are not fully understood.

In the *Hoxa3* mutant embryos, sensory neuronal precursor cells and Schwann cell-lineage NCCs of the IXth nerve are defective in their migration [10]. There is a report that hindbrain NCCs are required for proper migration of neuronal placode cells [19]. Importantly, mouse *Hoxa3* is expressed in both NCCs and placode cells at the prospective IXth nerve-forming area [10]. To address the cell autonomy of these NCCs and nerve precursor cells lacking Hoxa3 function, we suppressed HOXA3 function specifically in NCCs or placode cells by introducing anti-sense morpholino oligonucleotides (MO) into chicken embryos. The results obtained from these embryos were somewhat unexpected. By suppressing *HOXA3* function in placodal cells, we discovered that not only the placode-derived cells of the IXth nerve but also those of the VIIth and Xth nerve were defective in their migration and that the Xth nerve connection with the neural tube was not formed, indicating that cell-autonomous function of *HOXA3* in placodal cells was required for these events. We also found that *HOXA3* function in NCCs or other cells in the neural tube was also required for the migration of placodal cells of the VIIth and Xth nerves.

An additional interesting finding was the expression pattern of the chicken *HOXA3* gene. Usually *Hox* genes are recognized to specify body structures posterior to the r1/2 boundary. But recent studies revealed that some *Hox* genes are expressed in the head of vertebrates anterior to the expected *Hox*-expressing region [20, 21]. In this present study we also isolated chicken *HOXA3* cDNA and analyzed its expression pattern in the embryos. Expression of *HOXA3* was detected in the anterior head region by *in situ* hybridization and RT-PCR analyses, which location is very much anterior to that documented in previous reports.

Results

Expression of chicken *HOXA3* in the region anterior to r4/5 and in branchial arch 3

To examine *HOXA3* expression, we performed whole-mount *in situ* hybridization of chicken embryos. *HOXA3* mRNA was observed not only in the expected area from previously reported *Hoxa3* expression patterns in other species, i.e., the hindbrain posterior to the r4/5 boundary, the spinal cord, and mesenchymal tissues caudal to the branchial arch 2/3 boundary, but also in more anterior regions. At stage (st)-21 [22], the prominent anterior limit of intense signals in the neural tube was at the r4/5 boundary (Figure 1A-C, white arrowheads), but the lateral edge of r4 also had strong expression of *HOXA3* (Figure 1B,C,D, black arrows). *HOXA3* was also expressed in the posterior half of the second branchial arches (Figure 1B,E, black arrowheads), in addition to the 3rd and 4th branchial arches. This signal in the second branchial arches appeared faintly at st-20 (data not shown); but at st-21, intense signals were observed, in both ectodermal and mesodermal cells (Figure 1E, arrowhead).

To compare the expression pattern of mouse *Hoxa3* with that of chicken *HOXA3*, we performed *in situ* hybridization of mouse embryos. In 14-18-somite stage (E9.0) embryos, intense *Hoxa3* signals were observed in the neural tube posterior to the r4/5 boundary, in arch3, and in caudal part of the body (Figure 1F). Only faint expression of *Hoxa3* was observed in arch2. Likewise, weak signals were seen in the anterior part of the head; and their distribution pattern quite resembled that of NCCs. This pattern was slightly different in early chicken embryos (see Supplementary Figure 1). As shown in Supplementary Figure 1A, *in situ* hybridization signals of chicken *HOXA3* were obscure in the anterior head region. To confirm this observation, we performed RT-PCR analyses of RNA specimens from chicken and mouse embryos (Supplementary Figure 2). These RT-PCR analyses clearly showed that, even though low, there existed transcription of *HOXA3/Hoxa3* both in the anterior head region of both chicken and mouse embryos. The *HOXA3*/*Hoxa3* signals obtained by

RT-PCR and *in situ* hybridization were quite comparable between the anterior (A) and posterior (P) tissues, and were clearly not artifacts, as supported by the RT negative control results.

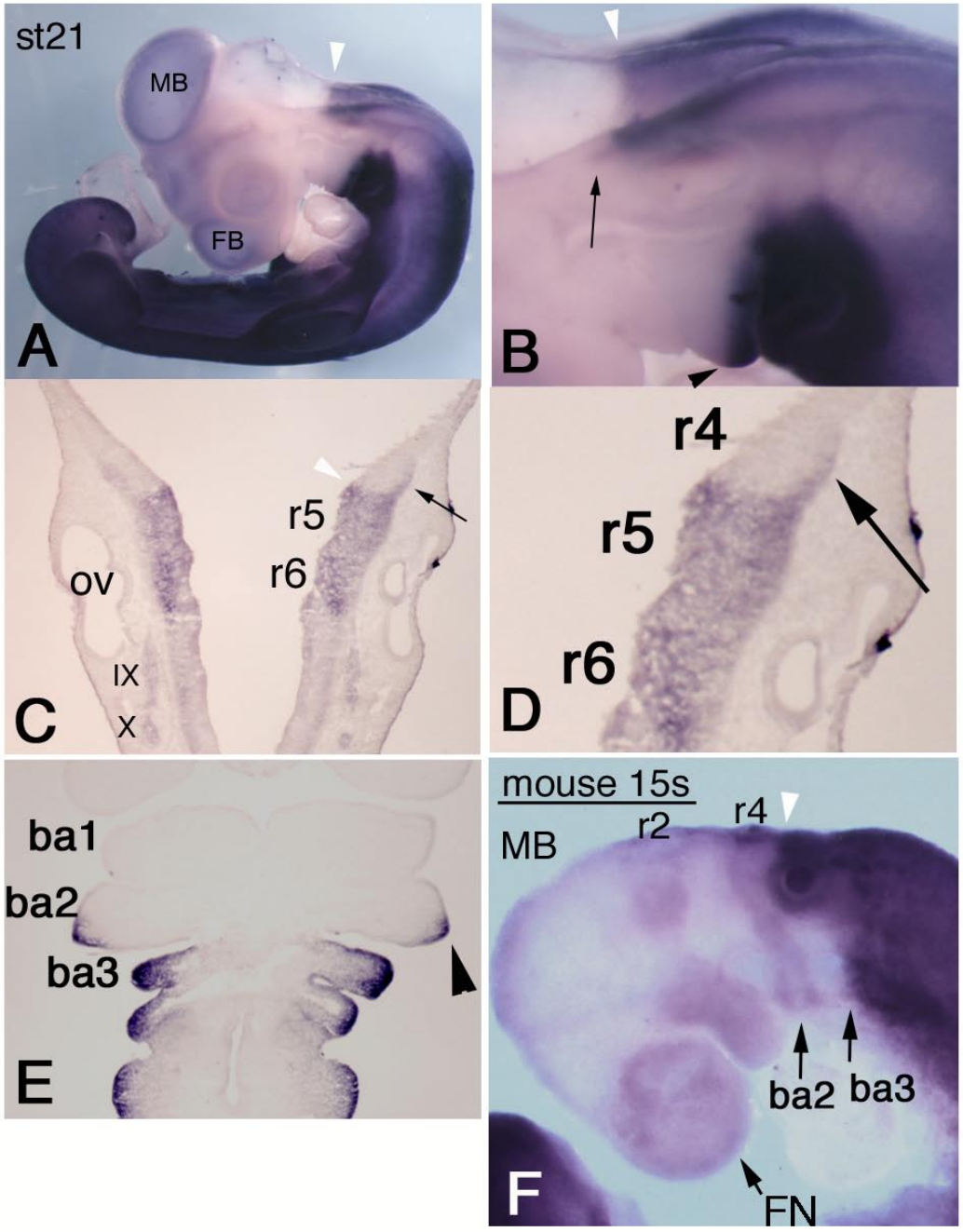

Figure 1: Expression pattern of chicken *HOXA3* and mouse *Hoxa3* in the anterior head region. *In situ* hybridization for *HOXA3* mRNA in a st-21 embryo (A-E). (A) Lateral view shows weak signals in midbrain (MB) and forebrain (FB). The white arrowhead shows the salient boundary at r4/5 in the hindbrain. (B,C,D) Black arrows indicate expression area at the lateral edge of r4. *HOXA3* expression is also observed in the posterior half of the second branchial arch (B,E, black arrowhead). (E) A frontal section of a st-21 embryo through the branchial arches. *HOXA3* expression is seen in the posterior half of the second branchial arch (arrowhead). ba1,2,3: branchial arches 1,2,3. (F) In this 15-somite-stage mouse embryo, weak *in situ* hybridization signals are detectable in neural crest cells from the midbrain (MB), r2, and r4 to the frontnasal region (FN) and branchial arches 2 (ba2) and 3 (ba3). The white arrowheads (B,C,F) indicate the r4/5 boundaries. Strong signals are seen in the neural tube posterior to the r4/5 boundary and in mesenchymal cells of branchial arch 3 and the more posterior region.

HOXA3 expression during branchial nerve development

We further examined *HOXA3* expression by focusing on the branchial nerve development. *In situ* hybridization performed on st-18 chicken embryos revealed strong signals along the IXth and Xth nerves (Figure 2A). To determine whether or not *HOXA3* was expressed in migrating precursor cells of the IXth and Xth nerves, as is the case for mouse *Hoxa3* [10], we examined earlier stages of embryos. At st-11, migrating neural crest cells from r6 seemed to express *HOXA3* (Figure 2B, arrowheads). At st-12, transverse sections through r6, 7, where the IXth and Xth nerve are forming, showed that NCCs and the neural tube expressed *HOXA3* (Figure 2F, white arrowheads).

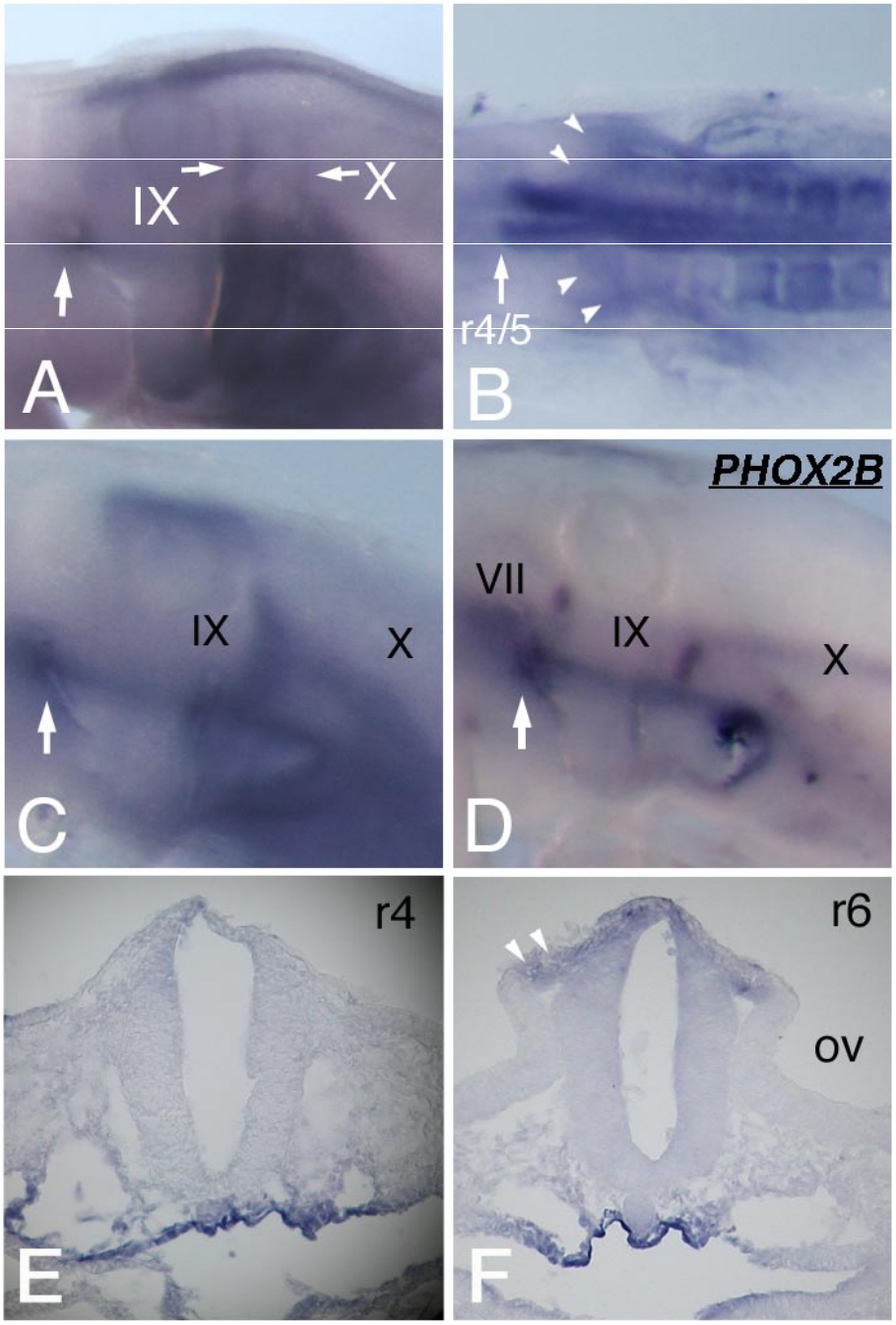

Figure 2: *HOXA3* expression during branchial nerve development. (A) At st-18 of chicken embryos, strong *HOXA3* expression along the IXth and Xth nerves is observed. The geniculate placode expresses *HOXA3* (large white arrow). (B) At st-11, *HOXA3* is expressed in the region posterior to the r4/5 boundary and in NCCs from r6 (arrowheads). *In situ* hybridization of st-15 embryos for *HOXA3* (C) and *PHOX2B* (D) shows that *HOXA3* is expressed in the area including placode-derived cells of the IXth and Xth nerve and in the geniculate placode (large white arrows). VII, IX, and X indicate the precursor cells of the VIIth, IXth, and Xth nerves, respectively. (E,F) Transverse sections of st-12 at r4 (E) and at r6 (F). At r4, *HOXA3* is weakly expressed with a slightly stronger signal in the dorsal region (E). At the r6 level, *HOXA3* signal is observed in the neural tube, and strongly in NCCs (F, arrowheads). OV, otic vesicle.

At st-15, compared with the distribution of cells bearing the placode-derived cell marker *PHOX2B* [24], *HOXA3* was expressed in the same region containing these placode-derived cells (Figure 2C,D). *In situ* hybridization of sections of st-20 embryos showed that *HOXA3* was expressed in the petrosal placode, from which distal ganglion neurons of the IXth nerve are derived (Figure 3A, bracket). Compared with glial cell-lineage marker *SOX10* [25, 26], *HOXA3* was also expressed all the way along the IXth nerve through the distal and proximal ganglia, the neural tube, and in NCCs populating the branchial arches (Figure

3A,D). At the Xth nerve level, again *HOXA3* was expressed along the Xth nerve fiber and in the region that included the distal ganglion (Figure 3B,C,E,F).

Besides being expressed in the IXth and Xth nerve precursor cells, *HOXA3* was also detected at the anterior dorsal end of the 2nd branchial arch of st-15 and -18 embryos (Figure 2A, C, arrows). ISLET-1 staining showed that this was the place from which placode-derived cells of the VIIth nerve delaminate to become mesenchymal cells (Figure 4C), suggesting that *HOXA3* was transiently expressed in the VIIth nerve distal ganglion precursor cells. This is an unexpected *HOXA3* expression area in light of previous reports. At st-12, sections through r4, where the VIIth nerve is forming, showed *HOXA3* mRNA expression in the neural tube with a slightly stronger signal in the dorsal region (Figure 2E). At the IXth and Xth nerve-forming area, NCCs expressed *HOXA3* more strongly than did the surrounding mesenchymal cells (Figure 2B,F). On the other hand, at the VIIth nerve-forming area, the expression level of *HOXA3* in NCCs seemed to be not stronger than that in the surrounding tissues (Figure 2E).

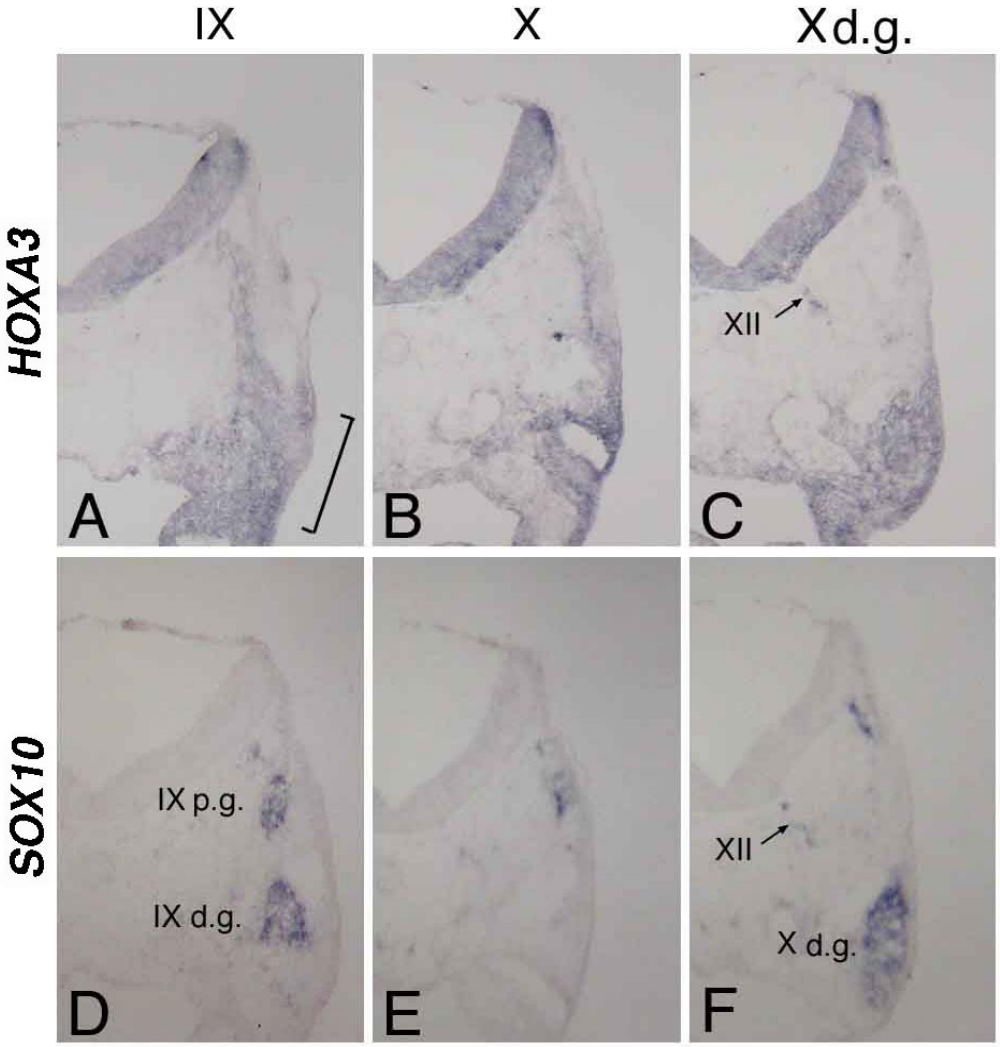

Figure 3: *In situ* hybridization for *HOXA3* (A,B,C) and *SOX10* (D,E,F) in sections made through the IXth (A,D) and Xth (B,E) nerve, and the distal ganglion of the Xth nerve (C,F). The bracket in "A" indicates the petrosal placode; XII in "C" and "F," the XIIth nerve; IXp.g. and IXd.g. in "D," the proximal and distal ganglion of the IXth nerve, respectively; and Xd.g. in "F," the distal ganglion of the Xth nerve.

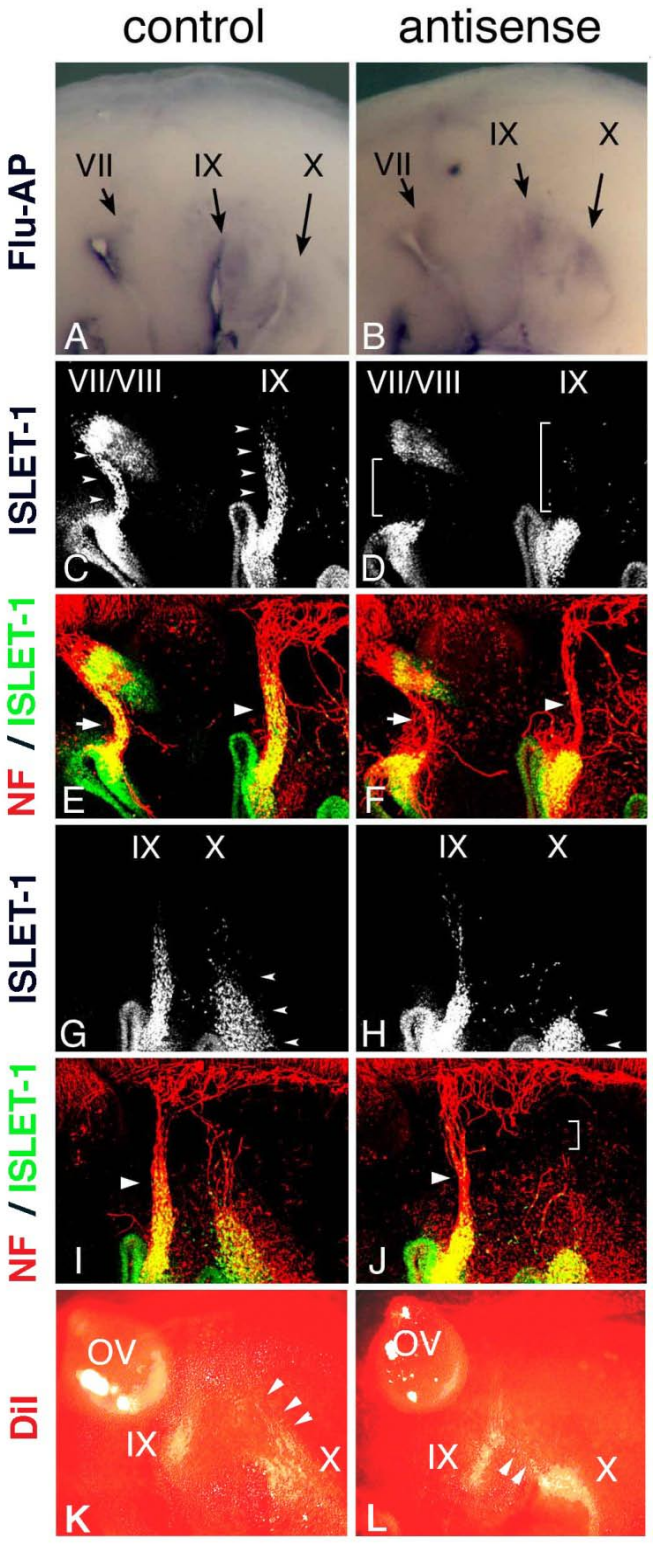

Figure 4: Electroporation of morpholino oligo into placode-derived cells. Control (A) or antisense (B) morpholino oligo are detected in placodes and placode-derived cells of the VIIth, IXth, and Xth nerves. Embryos electroporated with control (C,E,G,I) or antisense (D,F,H,J) Morpholino oligo were double-stained (E,F,I,J) for ISLET-1 (green) and neurofilaments (red); only single fluorescein images for ISLET-1 are shown in "C," "D," "G," and "H." In control embryos (C,G), placode-derived cells of the VIIth, IXth, and Xth nerve have migrated dorsally (small arrowheads); but in embryos electroporated with antisense oligo (D,H), the migration of these cells has been disrupted (D, brackets; H, small arrowheads). Neurofilament staining shows that in antisense oligo-containing embryos, the VIIth (arrow in "F") and IXth (large arrowhead in "F") nerve fibers are thinner than those of the control embryo (arrow and large arrowhead in "E") and that the Xth nerve connection to the neural tube has been affected (bracket in "J"). Large arrowheads in "I" and "J" indicate the IXth nerve fibers. (K,L) DiI-injected embryos after electroporation. In control embryos (K), placode-derived cells of the Xth nerve have migrated dorsally (arrowheads). In embryos electroporated with antisense MO (L), these cells didn't migrate dorsally, and some of them moved towards the placode-derived cells of the IXth nerve (arrowheads).

HOXA3 cell-autonomously regulates migration of the VIIth, IXth, and Xth nerve placode-derived cells

In *Hoxa3* knockout mouse embryos, placode-derived cells of the IXth nerve were affected in their dorsal migration, but whether cell-autonomous and/or non-cell autonomous function of *Hoxa3* is required for migration has not been determined [10]. To knockdown *HOXA3* function in placode-derived cells, we electroporated fluorescein-tagged *HOXA3* antisense morpholino oligo (MO, Gene Tools) into the ectodermal region that included all of the epibranchial placodes at st-9-11. For a control, MO having the inverse sequence of *HOXA3* antisense MO was used. MO sequence specificity was checked by BLAST searching of the chicken genome sequence database (NCBI, build 2.1). The antisense MO sequence perfectly matched only the *HOXA3* locus (data not shown). Electroporated control or antisense MO was detected with alkaline phosphatase-conjugated anti-fluorescein Fab fragment in the geniculate (VII), petrosal (IX), and nodose (X) placodes (Figure 4A,B). In control MO-electroporated embryos (n=16), anti-ISLET-1 immunostaining showed that placode-derived cells of the VIIth, IXth, and Xth nerve had migrated dorsally (Figure 4C,G, arrowheads). When antisense MO was electroporated into the placodes, the dorsal migration of all of these placode-derived cells was disrupted (Figure 4D,

brackets; H, L, arrowheads). In antisense MO-electroporated embryos, 7 samples out of 28 placode-derived cells of the VIIth nerve, 10/28 for the IXth nerve, and 17/28 for the Xth nerve were abnormal in their migration. These migration defects were confirmed directly by tracing placode-derived cells with a carbocyanine dye, DiI (Figure 4K,L, arrowheads). Double staining for ISLET-1 and neurofilaments showed that when the migration of placode-derived cells of the VIIth and IXth nerves was affected, the placode-derived cells were connected to the neural tube with a thinner bundle of neurofilaments than those in the control embryos (Figure 4E,F, arrows and arrowheads). On the other hand, when nodose placode-derived cells revealed a defect in migration, the nerve connection was thinner (n=13/28) than in the control embryos (n=16) or a gap was observed in the neurofilament signals between these cells and the neural tube (n=4/28, Figure 4H,J, small arrowheads and bracket). These results demonstrate that *HOXA3* cell-autonomously regulated the migration of the VIIth, IXth and Xth nerve placode-derived cells, and was required for normal connection of these cells to the neural tube.

HOXA3 function in the neural tube and/or neural crest cells is also required for migration of the placode-derived cells

Mouse and chicken *HOXA3* mRNAs are expressed in the NCCs associated with the IXth and Xth nerves; and in *Hoxa3* KO mouse embryos, NCCs along the IXth nerve show an abnormality in their migration to the distal ganglion [10]. Earlier it was reported that when the neural crest of chicken embryos was removed before the NCCs started their emigration, the migration of placode-derived cells did not occur, and the nerve connection to the neural tube failed to form [19]. To reveal the function of *HOXA3* in the neural tube and NCCs, we injected antisense MO into the chicken neural tube throughout the hindbrain of st-9-11 embryos, and electroporated them into the cells. Staining of st-14 embryos with anti-fluorescein Fab fragment and then with anti-HNK-1 (NCCs marker) antibody showed that MO had been successfully introduced into both the neural tube (data not shown) and NCCs in and towards branchial arches 2,3, and 4 (Figure 5A,B). When embryos were allowed to grow until st-19+, electroporated control and antisense MO were both distributed in the vicinity of the developing VIIth, IXth, and Xth nerves; and a substantial portion of the signals was seen near the distal ganglia and placode areas (Figure 5C,D). This finding indicates that some antisense MO-containing NCCs migrated towards the placodes. Since in *Hoxa3* KO mouse embryos, only some of the NCCs from r6 were affected in their migration [10, 12], there was a possibility that some of the NCCs containing antisense MO were abnormal. We performed *in situ* hybridization of MO-electroporated embryos to reveal the distribution pattern of *SOX10*-expressing neural crest cells, which fail to migrate toward the distal ganglion of the IXth nerve in *Hoxa3* KO mice [10]. In control embryos (n=12), *SOX10*-positive cells were associated with the VIIth, IXth, and Xth nerves (Figure 5E) at st19+. With antisense MO (n=18), *SOX10*-expressing NCCs also were observed along these nerves, indicating that these cells were migrating towards the distal ganglia (Figure 5F, arrowheads). Although NCCs surrounding the distal ganglia of the VIIth, IXth, and Xth nerves were expected to contain electroporated MO (see Figure 5C,D), we could not obtain concrete evidence that *HOXA3* cell-autonomously regulated NCCs migration towards the distal ganglia. But when antisense MO was electroporated, there was a difference in the distribution pattern of *SOX10*-experssing NCCs compared with that of the control embryos. Surprisingly, 9 out of 18 antisense MO-electroporated embryos had weaker signals between the distal ganglion of the VIIth nerve and the VIIIth nerve ganglion/neural tube (Figure 5F, bracket), although we could not detect as strong expression of *HOXA3* in NCCs derived from r4 (Figure 2E) as in those from r6 and 7. A low level of HOXA3 in NCCs from r4 may have functioned cell autonomously, or HOXA3 function in other cells of the neural tube might have regulated NCC distribution. In addition, *SOX10*-positive NCCs seemed to be less clearly separated into those along the IXth and Xth nerve (Figure 5F); for there were many diffuse signals between these nerves.

SOX10-expressing cells are expected to interact with placode-derived cells, which are migrating dorsally and extending their axons to the neural tube at this stage, so we next analyzed the phenotype of placode-derived cells in embryos with MO electroporated into the neural tube and NCCs at st-10-11. When embryos that had been electroporated with antisense MO were stained with anti-ISLET-1 and neurofilament antibody (n=16), the placode-derived cells of the VIIth nerve showed abnormalities in their dorsal migration (n=4/16, Figure 6A,B bracket); and the nerve connection between these cells and the neural tube was thinner than that in the control embryos (n=3/22, Figure 6C,D, arrows), as seen when antisense MO was electroporated into the placodes. Placode-derived cells of the Xth nerve also were affected in their dorsal migration when antisense MO was electroporated into the neural tube and NCCs (n=10/16, Figure 6E,F

arrowheads), and the nerve connection to the neural tube was disrupted (n=6/22 Figure 6G,H, bracket) or thinner (n=5/22). These results demonstrate that *HOXA3* function in the neural tube and/or NCCs was required for migration of the placode-derived cells of the VIIth and Xth nerves, and for the connection of these cells to the neural tube. On the other hand, regarding the IXth nerve, there was no or only a very subtle difference observed between antisense and control MO-electroporated embryos (n=16, Figure 6A-D, arrowheads).

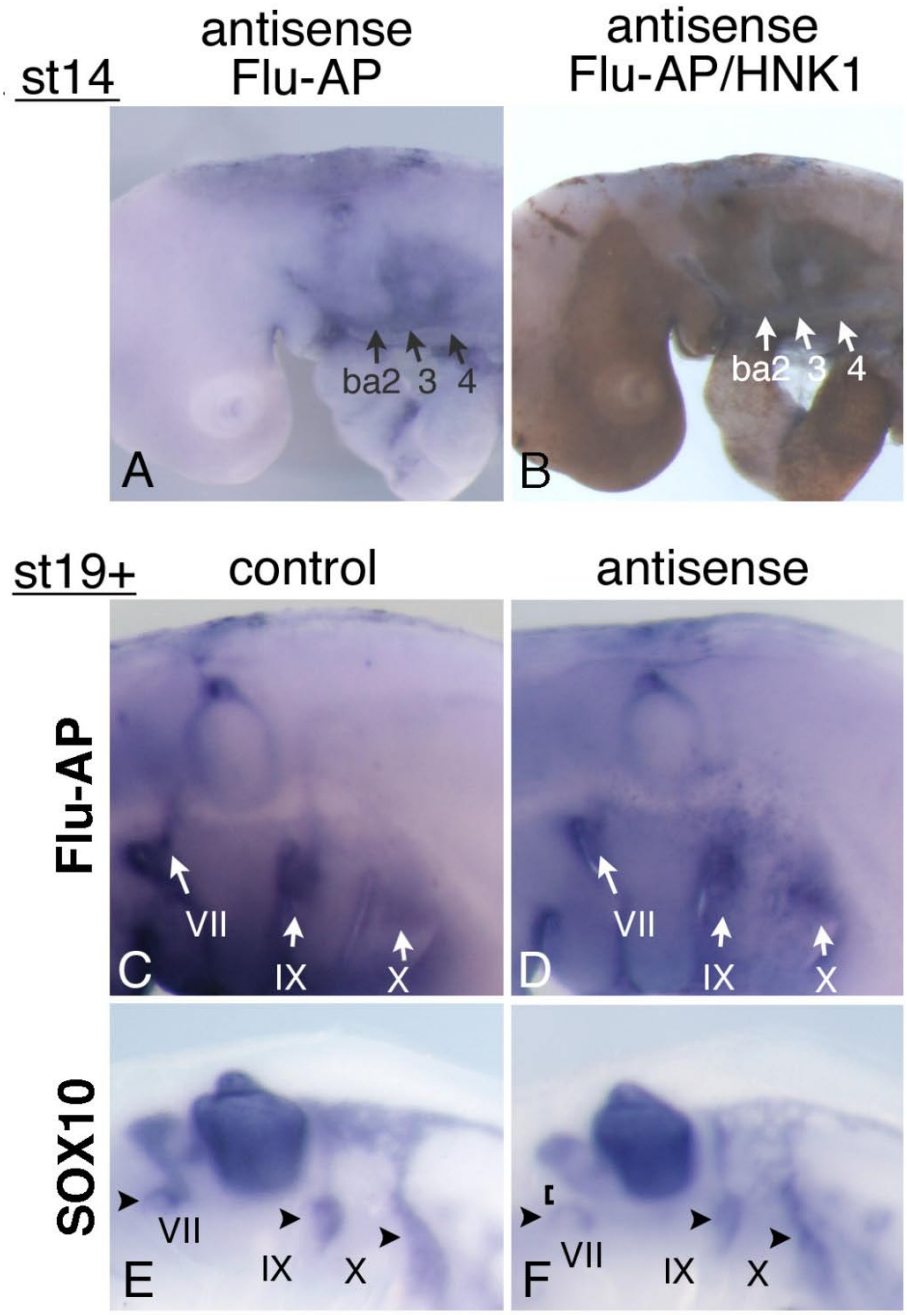

Figure 5: Electroporation of morpholino oligo into the neural tube and NCCs. (A) Antisense oligo is detected in the cellular streams to branchial arches 2,3, and 4 (ba2,3,4). (B) Staining for HNK-1 in the embryo shown in "A" confirms that these streams are NCCs. (C,D) At st-19+, control (C) or antisense (D) morpholino oligo is detected around the distal ganglia of the VIIth, IXth, and Xth nerves (arrows). (E,F) In embryos electroporated with control (E) or antisense (F) oligo, *SOX10*-expressing cells are observed around the distal ganglia of the VIIth, IXth, and Xth nerve (arrowheads). In "F," the VIIth nerve connection is disrupted (bracket).

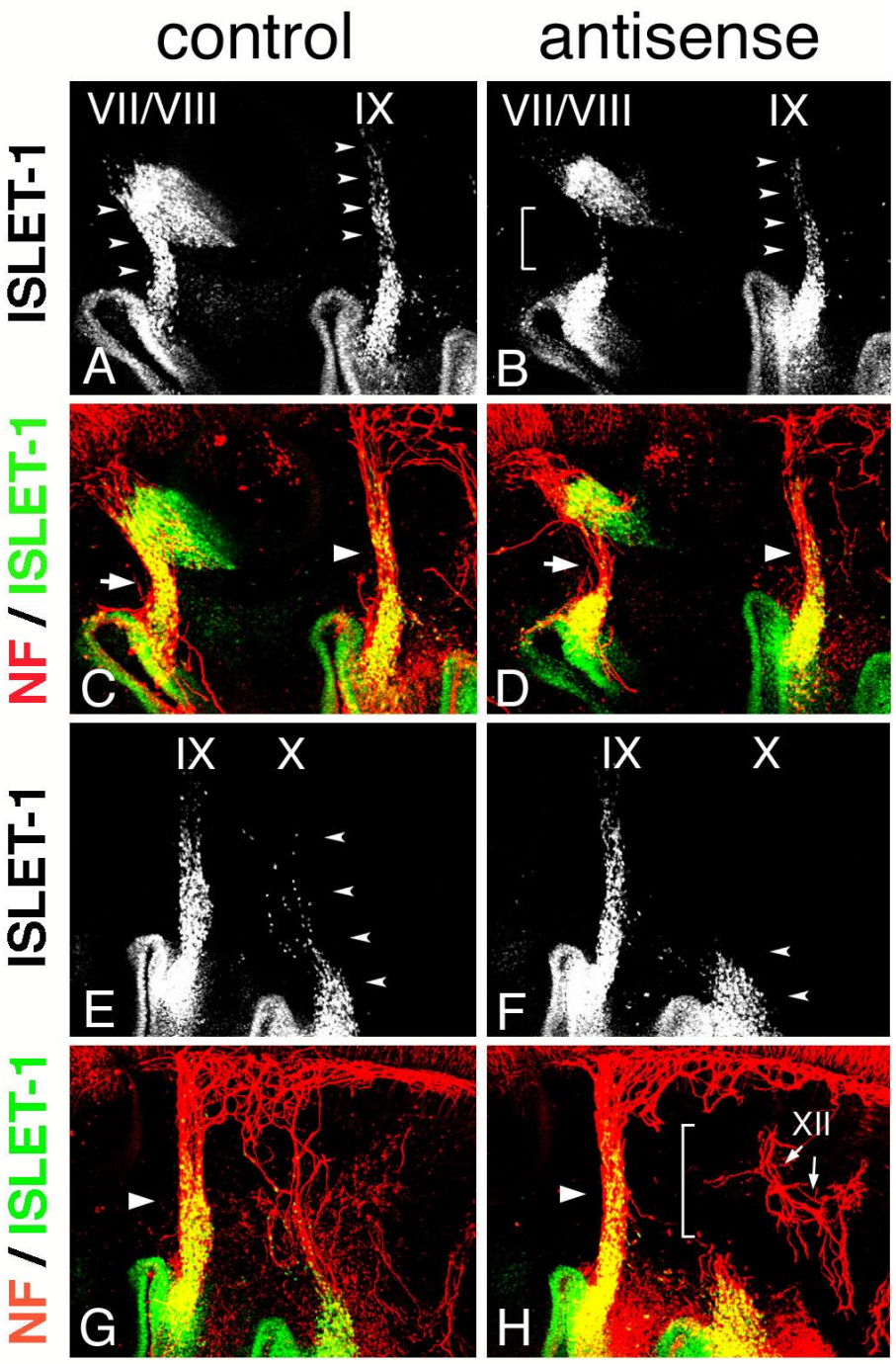

Figure 6: Electroporation of morpholino oligo into the neural tube and NCCs. Electroporation with control (A,C,E,G) or antisense (B,D,F,H) morpholino was performed, and embryos were stained for ISLET-1 and neurofilaments. Double fluorescence images (C,D,G,H) and single fluorescence ones for ISLET-1 (A,B,E,F) are shown. Dorsal migration of the placode-derived cells of the VIIth, IXth, and Xth nerves (arrowheads) is revealed (A,E), but migration is affected in placode-derived cells of the VIIth (bracket in "B") and Xth nerve (arrowheads in "F"). The VIIth nerve fiber in the embryo electroporated with antisense oligo (arrow in "D") is thinner than that in the control embryo (arrow in "C"), and the Xth nerve connection is disrupted (bracket in "H"). Large arrowheads (C,D,G,H) indicate the IXth nerve fiber. XII in "H" indicates the XIIth nerve.

Discussion

Expression of *HOXA3* anterior to r4/5 and to ba2/3 boundaries

It has been thought that *Hox* genes are involved in patterning of the embryonic body of vertebrates along the A-P axis in the area posterior to r1/2 [27]. NCCs from the hindbrain are also under the control of the "Hox code," by which NCCs are directed toward branchial arches 2, 3, and 4 express particular sets of *Hox* genes; however, branchial arch 1 has no *Hox* gene expression [27-29]. It was shown earlier that *Hoxa3*, along with other group 3 paralogous genes, is expressed in the region posterior to r4/5, in NCCs in branchial arch 3, and in more posterior regions of mouse embryos [9, 11, 30-32].

Here we found that chicken *HOXA3* and mouse *Hoxa3* were expressed in more anterior regions. *In situ* hybridization of 14-18-somite-stage mouse embryos showed weak *Hoxa3* expression in the region anterior to r4/5, very similar to NCCs' migration pattern. (Figure 1F). On the other hand, in chicken embryos, *HOXA3* expression in the anterior head region was obscure and seemed to be ubiquitous (Figure 1A, Supplementary Figure 1A,B,E,F). These expression patterns were consistent when several different *HOXA3* cDNA probes were used (data not shown). Thus the expression pattern of *HOXA3/Hoxa3* seems to be slightly different between chicken and mouse embryos in the anterior head region, although it is quite similar in the region posterior to r4/5. At a later stage, chicken *HOXA3* was also expressed in a restricted area at r4 and branchial arch2 (Figure 1B-E). RT-PCR analyses revealed that *HOXA3*/*Hoxa3* was definitely transcribed in the anterior head at various stages in chicken and mouse embryos (Supplementary Figure 2). The comparable signal of mouse *Hoxa3* mRNA in lateral r4 is recognizable in Figure 1 of the previous report by Gaufo et al. [33]. Further investigation of this *Hoxa3* expression in the lateral edge of r4 might be important. Electroporation of *HOXA3* antisense morpholino oligo (MO) resulted in migration defects in the placode-derived cells of the VIIth nerve (Figure 4D), indicating that chicken *HOXA3* function was required in the region anterior to the r4/5 boundary level.

Indeed, it was earlier reported that *Hoxa3* knockout mice showed some defects in the area anterior to the r4/5 boundary. For example, both maxilla and mandible, which are derived from NCCs in branchial arch 1, are altered in shape in *Hoxa3* knockout mice [11]. We found that mouse *Hoxa3* was expressed, although weakly, in branchial arch 1, which has been recognized as a *Hox*-negative default state under "*Hox* code" patterning, indicating that cell-autonomous function of *Hoxa3* may be required for proper development of these bones. In *Hoxa3* knockout mice, there were also defects in the zygomatic process of the squamosal bone, the thyroid diverticulum (thyroid precursor cells), and the VIIth nerve motor neurons, all of which are formed anterior to r4/5 [11, 12 and Watari-Goshima et al., unpublished results], suggesting that *Hoxa3* is probably involved in patterning various tissues in the anterior hindbrain level and in the more anterior region. From this point of view, our interpretation of the results obtained by Creuzet et al., [34], regarding the ectopic expression of *HOXA3* in the anterior head of chicken embryos, would be different from the authors'. The head defects they observed might not have been due to perturbation of a Hox-negative region with ectopic *HOXA3* expression, but rather to over-expression of HOXA3 perturbing the Hox code or stoichiometry among the Hox co-factors. Since *Drosophila* anterior HOM-C complex genes, such as *labial*, *proboscipedia*, and *deformed* specify the head segments, this kind of interpretation might be important [35, references therein].

It was earlier reported that other *Hox* genes are also expressed in previously thought Hox-negative regions. For example, *in situ* hybridization and immunostaining for *Hoxa2* and *Hoxd1* reveal expression in the diencephalon of mid- and late gestation stage embryos, suggesting that *Hox* genes may be involved in patterning this region [36]. In *Xenopus*, *Hoxa1* is expressed in a small number of neurons in the midbrain region [37]. Also in zebrafish embryos, *Hox* group 1 paralogs, *Hoxa1a* and *Hoxc1a*, are detected in some neurons that reside in the midbrain [38]. In addition, mouse *Hoxa1* is expressed more anterior to the ventral fore/midbrain boundary [21]. *Hoxb8* knockout mice show a defect in grooming behavior, which seems to have resulted from abnormalities in the central nervous system; and in adult mice, *Hoxb8* expression is observed in the olfactory bulb, hippocampus, cortex, cerebellum, and basal ganglia, etc. [20]. In considering these *Hox* gene expressions in the forebrain and midbrain with our findings of *Hoxa3* expression in non-neuronal tissues of the head region, further investigations on *Hox* gene functions in such regions should lead to new insights into the patterning of embryonic development by *Hox* genes.

Hoxa3 functions for branchial nerve development

Vertebrate branchial nerves, i.e., the Vth, VIIth, IXth, and Xth cranial nerves, have neural crest-derived and placode-derived sensory neurons in

their proximal and distal ganglia, respectively [18]. These nerves also have motor neurons, the cell bodies of which lie in the ventral hindbrain; and their axons project to the branchial arches through proximal and distal ganglia during development [39]. The sensory ganglia of these nerves are known to be weakly chemoattractive for motor neurons, as shown in co-culture experiments [40]. It is known that placode-derived neurons differentiate earlier than neural crest-derived ones [41, 42] and that in embryos where the placodes have been removed, the axonal projection pattern of proximal ganglion neurons to the periphery is defective [43]. These findings suggest that proper developmental regulation of the placode-derived neurons should be required for all 3 types of branchial nerve neurons, i.e., the 2 sensory types (neural crest-derived and placode-derived neurons) and the 1 motor type to project their axons correctly to their targets.

How are placode-derived neuronal precursor cells regulated? Previously it was reported that before neuronal precursor cells delaminate from the epibranchial placodes, NCCs have already reached just beneath the placodes and that these placode-derived cells then migrate along these NCCs [44]. Begbie and Graham [19] showed that in embryos the neural fold of which had been removed before NCC emigration from the neural tube, placode-derived neuronal cells failed to migrate and connect to the neural tube, indicating that NCCs and the dorsal part of the neural tube are required for these events. However, little is known about the molecular mechanisms regulating interactions among placode-derived cells, NCCs, and the neural tube.

We previously reported that in *Hoxa3* knockout mice, Schwann cell-lineage NCCs in the IXth nerve-forming area and placode-derived cells of the IXth nerve are defective in their migration [10]. As mouse *Hoxa3* is expressed in both NCCs and placode-derived cells at the IXth nerve level [10], in which cells *Hoxa3* function was required for migration had remained unknown. In this report, we showed that *HOXA3* regulated placode-derived cell migration both cell autonomously and non-cell autonomously.

The experiments in which *HOXA3* function was blocked in epibranchial placode-derived cells revealed that *HOXA3* was required for the migration of not only petrosal gangalion neurons (IXth) but also nodose (Xth) and geniculate (VIIth) ganglion ones (Figure 4). When anti-*HOXA3* antisense MO was electroporated at a little later stage (st-12), placode-derived cell migration defects were not observed (data not shown), suggesting that *HOXA3* function in pioneering cells may be essential for migration towards the neural tube.

There are a number of transcription factors that are known to play a role in the development of epibranchial placodes and placode-derived neurons. The basic helix-loop-helix (bHLH) transcription factor *neurogenin2* (*Ngn2*) and its downstream bHLH genes are required for neuronal cell fate determination and differentiation; and in *Ngn2* knockout mice, no neuronal precursor cells are observed to delaminate from the placodes [45]. In the chicken embryo, transcription factor *SOX3* is expressed in epibranchial placodes; and neuronal precursor cells leaving the placodes subsequently express *NGN1*, *NEUROD*, *NEUROM*, and *PHOX2A* [46]. *SOX3* over-expression in placodes causes the loss or a reduction in the number of placode-derived cells that migrate, suggesting down-regulation of *SOX3* to be important for placode cells to delaminate [46]. Depletion of *HOXA3* expression in the epibranchial placodes results in no apparent decrease in the number of delaminating cells, and placode-derived cells are detected with neuronal marker ISLET-1 [47]. Taken together, the data suggest that placodal cells are determined to acquire neuronal cell fate during delamination, and then need to be guided towards the neural tube by different mechanisms, in which *HOXA3* plays a role.

Depletion of *HOXA3* function in placodal cells led to failure of formation of the Xth nerve connection (Figure 4J). This situation resembles what we observed in *Hoxa3* knockout mice; in these mutants, when placode-derived cells of the IXth nerve fail to migrate near the lateral edge of the neural tube, these cells fail to send their axons to the neural tube [10]. This finding suggests that migration of placode-derived cells near the proximal ganglia or the entry point of the neural tube may be an important step for placode-derived neurons to send their axons centrally, and even for proximal ganglion neurons and motor neurons to project their axons into the periphery. On the other hand, when migration of the geniculate (VIIth) and petrosal (IXth) ganglion neurons was severely hampered by electroporation with antisense MO into the placodes (Figure 4D), these neurons still had connections to the neural tube; although the bundle was thinner than in the control MO-electroporated embryos (Figure 4F). This thin connection might have resulted from the residual activity of HOXA3 in these cells or alternatively, some non-cell autonomous function of *HOXA3* might have made it possible for the placode-derived cells to connect to the neural tube.

Electroporation of *HOXA3* antisense MO revealed that this gene was also required in NCCs and/or the neural tube for placode-derived cell mi-

gration. When antisense MO was electroporated into the neural tube and NCCs, the migration of the majority of NCCs towards the placodes seemed to have occurred normally (Figure 5B,F), but the placode-derived neuronal cell migration was disrupted (Figure 5B,F). As mentioned above, there are reports that placode-derived cells migrate along the NCCs [19, 44], suggesting that NCCs may give some information to placode-derived neurons for their migration towards the proximal ganglia. Taken together, the earlier findings and our present results indicate that *HOXA3* is required for placode-derived neurons to receive some guidance cue, and also for NCCs and/or the neural tube to provide them with such cue.

Knockout mice for several genes expressed in NCCs or the neural tube were reported to show abnormalities in their branichial nerve connections [48-51]. Among them, *Wnt1* and *Wnt3a* double knockout mice and mutants of beta-catenin, a wnt signaling pathway mediator, in which the gene function is eliminated in NCCs, show poorly formed connections of the IXth and Xth nerve [52, 53]. In addition to its suggested functions in survival and/or expansion of NCCs, the wnt signaling pathway might also be required for interaction of these cells with placode-derived cells. Interestingly, the epibranchial placodes of the chicken embryo express *cFz* genes, a family of putative Wnt receptors [54].

Mutations in the genes required for the maintenance of neural stem cells in the developing cranial ganglia are known to result in abnormal cranial nerve connections [55, 56]. Especially, *Hes1* and *Hes5* double-mutant mouse embryos show a glossopharyngeal nerve phenotype similar to that of the *Hoxa3* mutant embryos [55]. Besides *Hes* genes, knockout mouse embryos for *Sal13*, encoding a putative transcription factor, also show glossopharyngeal nerve and palate defects similar to those in *Hoxa3* mutants [57]. Inspecting genetic interactions between these genes and *Hoxa3* may be informative.

In embryos whose NCCs and neural tube had been electroporated with *HOXA3* antisense MO, more *SOX10*-positive NCCs were seen between the IXth and Xth nerve-forming areas (Figure 5F), and there were fewer *SOX10*-positive NCCs between the proximal and distal ganglia of the VIIth nerve (Figure 5F, bracket) than in control MO-electroporated embryos (Figure 5E). This observation may just reflect the defective migration and axon guidance of the placode-derived cells. However, there remains a possibility that *HOXA3* function in Schwann cell-lineage NCCs derived from r5 and more caudal areas was required for interaction with the developing nerve bundle of placode-derived cells.

In *Hoxa3* knockout mice, *Sox10*-positive NCCs fail to migrate towards the petrosal (IXth) ganglion and become stalled around the proximal ganglion-forming area [10]. Electroporation of NCCs and the neural tube with *HOXA3* antisense MO did not result in this severe defect. We electroporated fluorescein-tagged MO into 7 somite- to 13 somite-stage embryos; and at all stages anti-fluorescein antibody staining revealed that the antisense MO-electroporated NCCs had reached the branchial arches or the distal ganglion-forming area (Figure 5A,D). At this moment the possibility cannot be excluded that the residual HOXA3 function in the electroporated NCCs had been adequate for these cells to migrate beyond the proximal ganglion-forming region. On the other hand, as mesenchymal cells among which NCCs migrate also express *HOXA3*, this gene may also regulate NCC migration non-cell autonomously.

In this report, we demonstrated that *HOXA3* was involved in regulation of the migration of the VIIth nerve placode-derived cells besides that of the IXth and Xth nerve ones. In *Hoxa1* knockout (*Hoxa1* -/-) and in *Hoxa1* +/-*Hoxb1* -/- mice, the IXth and Xth nerve have no connection with the neural tube, and the nerve connection of the VIIth /VIIIth ganglion to the hindbrain is not always apparent [58, 59], suggesting that *Hoxa1* and *Hoxb1* are required for placode-derived neurons of all these nerves to connect with the hindbrain. When the above findings are taken together with the observation that the IXth nerve connection in *Hoxa3* knockout mice is disrupted [10], it would appear that multiple *Hox* genes are required for these events in the mouse embryo. It would be interesting to reveal whether placode-derived cells of all these nerves use the same cues to migrate and connect to the neural tube or not, and how *Hox* genes regulate them synergistically.

In the past decade, many studies have revealed various molecular mechanisms that are involved in cell and axon growth cone migration. Our knowledge is increasing with respect to the attractive and repulsive cues, their receptors, and downstream signaling molecules. Although in developing organisms it is essential that these molecules should be regulated appropriately, both in migrating cells and in the cells that guide them, little is known about what kinds of regulation are carried out, and what mechanisms can coordinate the activities of migrating cells and guiding cells. Regulation by a single transcription factor in both migrating cells and cells along the pathway may

be an important strategy to make them coordinate properly.

Materials and methods

Cloning of chicken *HOXA3* cDNA

A 25-somite stage-chicken cDNA library was screened with a chicken genomic *HOXA3* fragment. Isolated clones contained an open reading frame (ORF) encoding 413 amino acids. The nucleotide sequence of *HOXA3* cDNA is deposited in GenBank (Accession number AB111110).

In situ hybridization

Whole-mount *in situ* hybridization was performed essentially as described by Wilkinson [60]. Chicken and mouse embryos were hybridized with digoxigenin-labeled RNA probes at 70°C and 63°C, respectively. *In situ* hybridization for the sections was performed as described by Suzuki et al. [61], except that the embryos were hybridized with probes at 60°C. For *HOXA3* probe, a 0.97kb *Pst*I-*Eco*RI fragment of *HOXA3* cDNA was transcribed. For the *PHOX2B* probe, a 0.37kb fragment of *PHOX2B* cDNA [62] was used; and for the *SOX10* probe, the fragment amplified with the following primers was used: 5'AATGGCACTTGCCTGAGCACCTC3' (forward) and 5'CTCCGTGGCTGGTACTTGTAGTC3' (reverse). The antisense probe for mouse *Hoxa3* was previously described [10].

Sectioning

Embryos stained as whole mounts were refixed in 4% PFA/PBS for 4h at 4°C. They were then immersed in a graded series of sucrose solutions, frozen in Tissue-Tek OCT compound (Sakura Finetechnical Co.), and sectioned at 10 μm.

Immunohistochemistry

Double staining for ISLET-1 and neurofilaments and observation under a confocal microscope was performed as described previously [10]. For the secondary antibodies, Alexa488-conjugated anti-mouse IgG and Alexa594-conjugated anti-rabbit IgG (Molecular Probes) were used.

In ovo electroporation and detection of morpholino oligo

Eggs of st-9-11 embryos were windowed, and ink was injected beneath the embryos. Fluorescein-labeled *HOXA3* antisense morpholino oligo (MO, Gene Tools) and its inversion control oligo used were the following: 5'GTAGGTCGCTTTTTGCATTTC GTTG3' and 5'GTTGCTTTACGTTTTTCGCTGG ATG3', respectively. Before injection, 1 mM solution of MO was heated at 65°C for 5 min, and then the MO was injected under a fluorescence stereomicroscope into either the neural tube or the area between the vitelline membrane and the ectoderm at the hindbrain level. Square 100-ms pulse waves of 12 or 14V were applied 5 times at 900-ms intervals across the hindbrain region of embryos with 4-mm-spaced electrodes and a square wave generator (CUY21, BEX). After the embryos had been allowed to develop until st-14 or st-19+, we collected and fixed them in Bouin's solution for 2 hours at room temperature prior to detecting the electroporated MO. Following washes with 75% and 95% ethanol, the embryos were rehydrated with 0.5% TritonX-100 containing PBS (PBST), and then bleached in 1%H_2O_2 in PBST for 1 hour. These embryos were blocked with 10% heat-inactivated serum, and incubated with alkaline phosphatase-conjugated anti-fluorescein Fab fragment (Roche) at a 1/4000 dilution for 2 hours at 4°C. Color reactions were performed with BMpurple (Roche) for 2 hours at room temperature. For ISLET-1 and neurofilament double staining, electroporated embryos were harvested at st-19+ and fixed in cold 4%PFA-PBS for 1-2 hours.

DiI labeling

DiI (D-282, Molecular Probes), a carbocyanine dye saturated in dimethylformamide, was diluted 1/10 in 0.3 M sucrose solution. DiI solution was injected into the space between the amnion and ectoderm around the placodal area of embryos electroporated with MO into the placodes. Embryos were harvested at st-19+, refixed in 4% PFA/PBS overnight at 37°C, then immersed in a graded series of glycerol solutions up to 100%. Embryos were viewed under a fluorescence microscope.

Supplementary Material

Supplementary Figure 1
[http://www.biolsci.org/v07p0087s1.pdf]

Supplementary Figure 2
[http://www.biolsci.org/v07p0087s2.pdf]

Acknowledgements

We are grateful to A. Kuroiwa, K. Umesono, and C. Goridis, for the *HOXA3* genomic probe, chicken cDNA library, *PHOX2B* probe, respectively. We are grateful for members of the laboratory of M. Takeichi and S. Takada, and H. Hoshino for their discussion about this work, and technical advice on *in ovo* electroporation respectively. This study was supported by grants from the Ministry of Education, Science, Sports, and Culture of Japan. N. W-G. was a recipient

of a Fellowship of the Japan Society for the Promotion of Science for Young Scientists.

Conflict of Interests

The authors have declared that no conflict of interest exists.

References

1. Lawrence PA, and Morata G. Homeobox genes: their function in Drosophila segmentation and pattern formation. Cell 1994; 78: 181-189.
2. Scott MP. Vertebrate homeobox gene nomenclature. Cell 1992; 71: 551-553.
3. Lumsden A, and Krumlauf R. Patterning the vertebrate neuraxis. Science 1996; 274: 1109-1115.
4. Fraser S, Keynes R, and Lumsden A. Segmentation in the chick embryo hindbrain is defined by cell lineage restrictions. Nature 1990; 344: 431-435.
5. Lumsden A. The cellular basis of segmentation in the developing hindbrain. Trends Neurosci. 1990; 13: 329-335.
6. Krumlauf R. Evolution of the vertebrate Hox homeobox genes. Bioessays 1992; 14: 245-252.
7. Krumlauf R, Marshall H, Studer M, et al. Hox homeobox genes and regionalisation of the nervous system. J Neurobiol. 1993; 24: 1328-1340.
8. Krumlauf R. Hox genes in vertebrate development. Cell 1994; 78: 191-201.
9. Hunt P, Gulisano M, Cook M, et al. A distinct Hox code for the branchial region of the vertebrate head. Nature 1991; 353: 861-864.
10. Watari N, Kameda Y, Takeichi M, et al. Hoxa3 regulates integration of glossopharyngeal nerve precursor cells. Dev Bio. 2001; 240: 15-31.
11. Chisaka O, and Capecchi MR. Regionally restricted developmental defects resulting from targeted disruption of the mouse homeobox gene hox-1.5. Nature 1991; 350: 473-479.
12. Manley NR, and Capecchi MR. The role of Hoxa-3 in mouse thymus and thyroid development. Development 1995; 121: 1989-2003.
13. Manley NR, and Capecchi MR. Hox group 3 paralogous genes act synergistically in the formation of somitic and neural crest-derived structures. Dev Bio. 1997; 192: 274-288.
14. Kameda Y, Nishimaki T, Takeichi M, et al. Homeobox gene hoxa3 is essential for the formation of the carotid body in the mouse embryos. Dev Bio. 2002; 247: 197-209.
15. Kameda Y, Watari-Goshima N, Nishimaki T, et al. Disruption of the Hoxa3 homeobox gene results in anomalies of the carotid artery system and the arterial baroreceptors. Cell Tissue Res. 2003; 311: 343-352.
16. Kameda Y, Arai Y, Nishimaki T, et al. The role of Hoxa3 gene in parathyroid gland organogenesis of the mouse. J Histochem Cytochem. 2004; 52: 641-651.
17. Chisaka O, and Kameda Y. Hoxa3 regulates the proliferation and differentiation of the third pharyngeal arch mesenchyme in mice. Cell Tissue Res. 2005; 320: 77-89.
18. D'Amico-Martel A, and Noden DM. Contributions of placodal and neural crest cells to avian cranial peripheral ganglia. Am J Anat. 1983; 166: 445-468.
19. Begbie J, and Graham A. Integration between the epibranchial placodes and the hindbrain. Science 2001; 294: 595-598.
20. Greer JM, and Capecchi MR. Hoxb8 is required for normal grooming behavior in mice. Neuron 2002; 33: 23-34.
21. McClintock JM, Jozefowicz C, Assimacopoulos S, et al. Conserved expression of Hoxa1 in neurons at the ventral forebrain/midbrain boundary of vertebrates. Dev Genes Evol. 2003; 213: 399-406.
22. Hamburger V, and Hamilton HL. A series of normal stages in the developement of the chick embryo. J. Morphol. 1951; 88: 49-92.
23. Su D, Ellis S, Napier A, et al. Hoxa3 and pax1 regulate epithelial cell death and proliferation during thymus and parathyroid organogenesis. Dev Bio. 2001; 236: 316-329.
24. Pattyn A, Morin X, Cremer H, et al. The homeobox gene Phox2b is essential for the development of autonomic neural crest derivatives. Nature 1999; 399: 366-370.
25. Cheng Y, Cheung M, Abu-Elmagd MM, et al. Chick sox10, a transcription factor expressed in both early neural crest cells and central nervous system. Brain Res Dev Brain Res. 2000; 121: 233-241.
26. Britsch S, Goerich DE, Riethmacher D, et al. The transcription factor Sox10 is a key regulator of peripheral glial development. Genes Dev. 2001; 15: 66-78.
27. Cobourne MT. Construction for the modern head: current concepts in craniofacial development. J Orthod. 2000; 27: 307-314.
28. Hunt P, Wilkinson D, and Krumlauf R. Patterning the vertebrate head: murine Hox 2 genes mark distinct subpopulations of premigratory and migrating cranial neural crest. Development 1991; 112: 43-50.
29. Trainor PA, and Krumlauf R. Patterning the cranial neural crest: hindbrain segmentation and Hox gene plasticity. Nat Rev Neurosci. 2000; 1: 116-124.
30. Gaunt SJ, Miller JR, Powell DJ, et al. Homeobox gene expression in mouse embryos varies with position by the primitive streak stage. Nature 1986; 324: 662-664.
31. Gaunt SJ. Homeobox gene Hox-1.5 expression in mouse embryos: earliest detection by in situ hybridization is during gastrulation. Development 1987; 101: 51-60.
32. Gaunt SJ. Mouse homeobox gene transcripts occupy different but overlapping domains in embryonic germ layers and organs: a comparison of Hox-3.1 and Hox-1.5. Development 1988; 103: 35-144.
33. Gaufo OG, Wu S, and Capecchi MR. Contribution of Hox genes to the diversity of the hindbrain sensory system. Development 2003; 131: 1259-1266.
34. Creuzet S, Couly G, Vincent C, et al. Negative effect of Hox gene expression on the development of the neural crest-derived facial skeleton. Development 2002; 129: 4301-4313.
35. Hughes CL and Kaufman TC. Hox genes and the evolution of the arthropod body plan. Evolution & Development 2002; 4: 459-499.
36. Wolf LV, Yeung JM, Doucette JR, et al. Coordinated expression of Hoxa2, Hoxd1 and Pax6 in the developing diencephalon. Neuroreport. 2001; 12: 329-333.
37. Kolm PJ, and Sive HL. Regulation of the Xenopus labial homeodomain genes, HoxA1 and HoxD1: activation by retinoids and peptide growth factors. Dev Bio. 1995; 167: 34-49.
38. McClintock JM, Carlson R, Mann DM, et al. Consequences of Hox gene duplication in the vertebrates: an investigation of the zebrafish Hox paralogue group 1 genes. Development 2001; 128: 2471-2484.
39. Lumsden A, and Keynes R. Segmental patterns of neuronal development in the chick hindbrain. Nature 1989; 337: 424-428.
40. Caton A, Hacker A, Naeem A, et al. The branchial arches and HGF are growth-promoting and chemoattractant for cranial motor axons. Development 2000; 127: 1751-1766.
41. D'Amico-Martel A, and Noden DM. An autoradiographic analysis of the development of the chick trigeminal ganglion. J Embryol Exp Morphol. 1980; 55: 167-182.
42. D'Amico-Martel A. Temporal patterns of neurogenesis in avian cranial sensory and autonomic ganglia. Am J Anat. 1982; 163: 351-372.

43. Hamburger V. Experimental analysis of the dual origin of the trigeminal ganglion in the chick embryo. J. Exp. Zool. 1961; 148: 91-124.
44. Ayer-Le Lievre CS, and Le Douarin NM. The early development of cranial sensory ganglia and the potentialities of their component cells studied in quail-chick chimeras. Dev Bio. 1982; 94: 291-310.
45. Fode C, Gradwohl G, Morin X, et al. The bHLH protein NEUROGENIN 2 is a determination factor for epibranchial placode-derived sensory neurons. Neuron 1998; 20: 483-494.
46. Abu-Elmagd M, Ishii Y, Cheung M, et al. cSox3 expression and neurogenesis in the epibranchial placodes. Dev Bio. 2001; 237: 258-269.
47. Pfaff SL, Mendelsohn M, Stewart CL, et al. Requirement for LIM homeobox gene Isl1 in motor neuron generation reveals a motor neuron-dependent step in interneuron differentiation. Cell 1996; 84: 309-320.
48. Gassmann M, Casagranda F, Orioli D, et al. Aberrant neural and cardiac development in mice lacking the ErbB4 neuregulin receptor. Nature 1995; 378: 390-394.
49. Meyer D, and Birchmeier C. Multiple essential functions of neuregulin in development. Nature 1995; 378: 386-390.
50. Erickson SL, O'Shea KS, Ghaboosi N, et al. ErbB3 is required for normal cerebellar and cardiac development: a comparison with ErbB2-and heregulin-deficient mice. Development 1997; 124: 4999-5011.
51. Qiu Y, Pereira FA, DeMayo FJ, et al. Null mutation of mCOUP-TFI results in defects in morphogenesis of the glossopharyngeal ganglion, axonal projection, and arborization. Genes Dev. 1997; 11: 1925-1937.
52. Ikeya M, Lee SM, Johnson JE, et al. Wnt signalling required for expansion of neural crest and CNS progenitors. Nature 1997; 389: 966-970.
53. Brault V, Moore R, Kutsch S, et al. Inactivation of the beta-catenin gene by Wnt1-Cre-mediated deletion results in dramatic brain malformation and failure of craniofacial development. Development 2001; 128: 1253-1264.
54. Stark MR, Biggs JJ, Schoenwolf GC, et al. Characterization of avian frizzled genes in cranial placode development. Mech Dev. 2000; 93: 195-200.
55. Hatakeyama J, Sakamoto S, and Kageyama R. Hes1 and Hes5 regulate the development of the cranial and spinal nerve systems. Dev Neurosci. 2006; 28: 92-101.
56. McNeill EM, Roos KP, Moechars D, et al. Nav2 is necessary for cranial nerve development and blood pressure regulation. Neural Dev. 2010; 5: 6.
57. Parrish M, Ott T, Lance-Jones C, et al. Loss of the Sall3 gene leads to palate deficiency, abnormalities in cranial nerves, and perinatal lethality. Molec Cell Biol. 2004; 24: 7102-7112.
58. Chisaka O, Musci TS, and Capecchi MR. Developmental defects of the ear, cranial nerves and hindbrain resulting from targeted disruption of the mouse homeobox gene Hox-1.6. Nature 1992; 355: 516-520.
59. Gavalas A, Studer M, Lumsden A, et al. Hoxa1 and Hoxb1 synergize in patterning the hindbrain, cranial nerves and second pharyngeal arch. Development 1998; 125: 1123-1136.
60. Wilkinson DG. Whole-mount *in situ* hybridization of vertebrate embryos. In: Wilkinson DG, ed. *In situ* Hybridization: A Practical Approach. Oxford: IRL Press; 1992: 75-83.
61. Suzuki SC, Inoue T, Kimura Y, et al. Neuronal circuits are subdivided by differential expression of type-II classic cadherins in postnatal mouse brains. Mol Cell Neurosci. 1997; 9: 433-447.
62. Stanke M, Junghans D, Geissen M, et al. The Phox2 homeodomain proteins are sufficient to promote the development of sympathetic neurons. Development 1999; 126: 4087-4094.
63. Johansson BM, and Wiles MV. Evidence for involvement of activin A and bone morphogenetic protein 4 in mammalian mesoderm and hematopoietic development. Mol Cell Bio. 1995; 15: 141-151.
64. Kuratani SC, and Kirby ML. Initial migration and distribution of the cardiac neural crest in the avian embryo: an introduction to the concept of the circumpharyngeal crest. Am J Anat. 1991; 191: 215-227.